

**Using tendency errors
to tune the parameterisation
of unresolved dynamical scale interactions
in atmospheric general circulation models**

Eigil Kaas, Annette Guldborg and Wilhelm May,

Danish Meteorological Institute, Lyngbyvej 100, DK-2100 Copenhagen, Denmark,

Michel Déqué,

Météo-France CNRM/GMGEC/EAC, 42 Avenue Coriolis, 31057 Toulouse Cedex 01, France

Corresponding author: Eigil Kaas, ek@dmi.dk, phone +45 3915 7424, fax +45 3915 7460

For this document is used Word 97 for Windows.

Manuscript submitted to

Tellus

1 October 1998

In revised form 19 February 1999

In final form 17 June 1999

Abstract

A parameterisation of non-linear dynamical interactions with unresolved scales is needed in most atmospheric models to ensure realistic fluxes of energy and enstrophy near and at the truncation limit.

In this paper a minimisation of tendency errors in low to medium resolution versions of the ARPEGE/IFS and the ECHAM4 general circulation models is sought in order to obtain spectral *empirical interaction functions* (EIFs) to be used in the formulation of horizontal diffusion. The tendency errors are calculated relative to high resolution adiabatic versions of the models themselves, meaning that the EIFs reflect all non-linear adiabatic processes.

Different EIFs are obtained for vorticity, divergence and temperature. The most striking feature is that the vorticity and temperature EIFs have non-negligible negative values for low wave numbers in large parts of the troposphere. This implies that these waves are enhanced in amplitude due to non-linear interactions with unresolved scales. For low resolution models the generation/dissipation of kinetic energy due to the interactions is not well parameterised by either the standard horizontal diffusion in the models, or the EIFs computed here.

When the EIFs are used in the formulation of horizontal diffusion it is seen that the kinetic energy spectrum is closer to observations than in the original model versions. Furthermore, the large scale systematic model errors are reduced in a medium resolution simulation, while less clear improvement is seen in a simulation at low resolution.

It is argued that the technique used in this paper is quite general and may be used to develop a more realistic parameterisation of unresolved dynamical scale interactions. The method should, with some modifications, also be applicable in semi-Lagrangian spectral models and in grid point models.

1. Introduction.

Since the governing atmospheric equations are highly non-linear, models based on these equations need a parameterisation - usually represented by horizontal diffusion (HD) - of the effects of dynamical interactions with scales not resolved in the models (e.g. Laursen and Eliassen, 1989; Koshyk and Boer, 1995 (KB)). HD is, however, also used for other purposes such as suppression of noise associated with numerical dispersion or inaccuracy in grid point models, and generally to avoid unrealistic reflection of vertically propagating gravity waves at the model top. Furthermore, if severe noise or instability related to interaction between model dynamics and the parameterised processes is detected, strong HD is in practice often used as a "panic" solution. The first motivation for HD, is different in character, because it is a parameterisation of an important physical process while the others are related to insufficient algorithms and formulations.

The dynamical scale interactions in the atmosphere lead to transfers of energy and enstrophy between different scales (Boer and Shepherd, 1983; KB). These transfers are similar to those seen in two dimensional turbulence (Kraichnan, 1967; Leith, 1968), which is characterised by an enstrophy cascading inertial subrange, i.e., a constant downscale flux of enstrophy, and a kinetic energy spectrum with a -3 slope. KB calculated the spectral fluxes associated with enstrophy and the rotational part of kinetic energy using a variety of assimilated data sources, and found no observational evidence of an enstrophy cascading inertial subrange since the enstrophy flux varies considerably with wave number. In spite of this variation, a ~ -3 slope of the energy spectrum, which is typical for two dimensional turbulence, is clearly seen in observations as shown by Wiin-Nielsen (1967), Boer and Shepherd (1983) and many others. This slope is a very robust feature of the atmospheric flow, which should be simulated by general circulation models (GCMs) at any reasonable horizontal resolution. Fortunately, HD in GCMs can ensure reasonable agreement with observed flow concerning the -3 slope and furthermore, a well tuned and formulated HD can reduce the systematic errors somewhat in medium to low resolution GCMs (KB; Laursen and Eliassen, 1989). Except for KB, however, little effort has been put into ensuring correct fluxes of energy and enstrophy in modern medium resolution GCMs.

Several investigations have generally shown reduced systematic errors as model horizontal resolution increases, e.g. Boville (1991), Boyle (1993), Déqué and Piedelievre (1995), Stendel and Roeckner (1998). Many high resolution models tend to have stronger westerlies at mid-latitudes than the corresponding low resolution model versions. This difference is often quite clear over the Southern Hemisphere (SH) where the subpolar trough is much too weak and its position shifted equatorward in low resolution models (Stendel and Roeckner, 1998). As an illustration of this, Fig. 1 shows the difference in mean sea level pressure (MSLP) in January between two simulations (to be described later) with high (T106) and low (T30) spectral model truncation. In both simulations the orography was truncated at T30 meaning that the structures in Fig. 1 are only related to different behaviour of the parameterised processes - *including* HD - at the different horizontal resolutions. One may thus speculate that inadequate HD at T30 could be responsible for some of the differences in Fig. 1. Note here, that we are not comparing with observations as the "truth" because we want to isolate to the extent possible the effect of the unresolved horizontal scale interactions. Thus, we are not interested in other sources of model errors which none deliberately may have been tuned to cancel the effect of the unresolved scale interactions.

Following KB but using a slightly different notation the tendency of the kinetic energy of the flow can be written

$$\frac{\partial E_n}{\partial t} = I_n + S_n \quad (1)$$

where I_n represents the non-linear exchange of kinetic energy between total wave number n and all other wave numbers and S_n includes all sources/sinks of kinetic energy, to which the (purely dynamical) conversion of potential to kinetic energy is an important contribution in this context. Since spectral atmospheric models have limited horizontal truncation n_* , the interaction term can be split into two terms

$$I_n = I_n^R + I_n^U \quad (2)$$

where I_n^R represents non-linear interactions with resolved wave numbers ($n \leq n_*$) and I_n^U interactions with unresolved wave numbers ($n > n_*$). KB were inspired by previous work of Leith (1971) to parameterise I_n^U in a spectral model by an expression of the form

$-2h_n E_n$ where h_n is some scale dependent interaction function. KB used ECMWF^a data assimilated at a horizontal truncation of T213 to estimate monthly means of I_n and E_n and obtained I_n^R from an $n_*=32$ truncation of the T213 data. An empirical approximation \hat{h}_n of h_n could then be isolated from (2):

$$\hat{h}_n = \frac{I_n^R - I_n}{2E_n} \quad (3)$$

Note that n_* was not assumed to fall in an enstrophy cascading inertial sub-range as assumed by Leith (1971). KB estimated \hat{h}_n from the rotational part of the flow and for non-linear interactions of enstrophy and kinetic energy only, but they assumed its validity as general interaction parameter (h_n) in the parameterisation of unresolved scale interactions for all prognostic variables:

$$\frac{\partial \Psi_{n,m}}{\partial t} = T_{n,m} - h_n \Psi_{n,m} \quad (4)$$

where $\Psi_{n,m}$ indicates either vorticity, divergence, temperature, surface pressure or humidity, $T_{n,m}$ tendencies of resolved linear and non-linear processes including the parameterised processes and index m the zonal wave number.

In the present paper the ideas in KB will be pursued by estimating vertically varying EIFs in two spectral atmospheric GCMs (ARPEGE/IFS and ECHAM4), which both employ an Eulerian formulation of the advection processes as in the model studied by KB. Both models currently use a damping that is a function of model level and total wave number n to parameterise unresolved scale interactions. Our EIF is obtained from tendency errors at low to medium model resolutions relative to high resolution model generated data sets. Our work is basically different from KB since different interaction functions are calculated and evaluated for vorticity, divergence and temperature, and not only the rotational part of the flow is used for these calculations. Furthermore, the new EIFs reflect all unresolved dynamical scale interactions, not only those associated with horizontal advection as in KB.

The organisation of the paper is as follows. Section 2 gives a brief overview of ARPEGE/IFS and ECHAM4 and in section 3 the methodology and the technique used

^a European Center for Medium Range Weather Forecasts.

to calculate the model tendency errors due to scale interactions is described. The results in terms of the EIFs are given in section 4, while section 5 describes the impact of using the EIFs in the formulation of HD in climate simulations. Finally, section 6 concludes the paper with a summary and discussion of the results.

2. Models

The French community climate model ARPEGE/IFS (Déqué et al., 1994), version 2, is one of the two GCMs applied in this study. The model solves the primitive equations using the spectral transform technique, Eulerian advection, and a three-level semi-implicit time stepping scheme. Normally version 2 has 41 sigma-pressure hybrid levels, but in this study a 31-level version has been adapted. The 31 levels shown in Fig. 2a are the same as the 31 levels used in the ECMWF re-analyses.

The dynamical core of the ECHAM4 model is quite similar to that of ARPEGE, while the physical parameterisation schemes are different (Roeckner et al., 1996). There are 19 vertical hybrid levels in the standard version of ECHAM4 which we use (Fig. 2b).

In both models the horizontal diffusion is applied as described in equation (4), but for temperature a hydrostatic correction is made in mountainous regions. The effect of this correction is taken into account in the EIFs, which for ARPEGE were calculated for three different horizontal resolutions: T21, T30 and T42 and for ECHAM4 at T30, only. The high resolution adiabatic model version used for determining tendency errors as described in section 3 was for both GCMs truncated at T106. Using two different GCMs allows an independent check of the results and reduces the risk of coding and implementation errors.

3. Methodology and calculation of tendency errors

As mentioned in the introduction the basic idea of the paper is to minimise tendency errors - or differences - between high and low resolution model versions at each model level. In other words we try to explain as much as possible of the tendency errors by a term of the form $h_n \cdot \Psi_{n,m}$ as in (4) and then use this term in the re-tuned model. In practice we first estimate the tendency errors and then use a simple linear least square fitting between the time series of tendency errors ($R_{n,m}(t)$) and the relevant prognostic variable ($\Psi_{n,m}(t)$) to obtain an empirical value ($\hat{h}_{n,m}$) of the interaction function, which is valid for each total and zonal wave number:

$$R_{n,m}(t) \approx -\hat{h}_{n,m} \Psi_{n,m}(t) \quad (5)$$

The regression includes both real and imaginary parts of the expansion coefficients which are merged into one long time series. The final EIF \hat{h}_n , valid for each total wave number, is obtained as a weighted average of the regression results $\hat{h}_{n,m}$ from the relevant zonal wave numbers. The weighting coefficient $w_{n,m}$ is defined as a fraction having the variance of $(\Psi_{n,m}(t))$ in the numerator. The denominator is determined as the mean of the squared distance between $R_{n,m}(t)$ and the fitted value $R_0 - \hat{h}_{n,m} \Psi_{n,m}(t)$, where R_0 and $\hat{h}_{n,m}$ are the fitting parameters. \hat{h}_n is then obtained as $\left(\sum_{m=0}^n w_{n,m} \hat{h}_{n,m} \right) / \left(\sum_{m=0}^n w_{n,m} \right)$. The weighting is only introduced to smooth the EIFs, but for the EIFs plotted in this paper - based on long simulations - the weighting has very little influence on the results. Furthermore, to avoid problems with noisy $\hat{h}_{n,m}$ values for low wave numbers, a simple damping of the amplitude of \hat{h}_n is introduced. The damping, which only is active for $n \leq 4$ consists of multiplying \hat{h}_n by $1/(6-n)^2$. It is motivated by low significance in the regression results for these wave numbers which, again, is due to long temporal variations relative to the length of the time series of $R_{n,m}(t)$ and $\Psi_{n,m}(t)$.

Calculating tendency errors of a GCM relative to a reference model or data set is not a trivial exercise. This is mainly because, having calculated a tendency difference between the model and the reference data, it is difficult to separate this difference into the "true" tendency error on the one side and the fraction which is related to initial dynamical gravity wave noise and to processes related to moisture spin-up on the other. To avoid some of these problems we have therefore - as in Jeuken et al. (1996) - performed a simple 4-dimensional assimilation - "nudging" - of the (truncated) reference data. In the nudging procedure the model is forced towards the reference data via a Newtonian relaxation term:

$$\Psi_{n,m}(t + \Delta t) = \Psi_{n,m}^*(t + \Delta t) + 2\Delta t \frac{(\Psi_{n,m}^{REF}(t + \Delta t) - \Psi_{n,m}(t + \Delta t))}{\tau} \quad (6)$$

where Δt is the length of the time step, the upper index * denotes the preliminary prognostic variable just before nudging, upper index *REF* indicates the variable the model is being relaxed towards, and τ is the relaxation time. Note, that the factor $2\Delta t$ in

(6) shows that a 3 time level time stepping scheme is used in our models (ARPEGE and ECHAM4) and that a $1\Delta t$ must be used for 2 level forward in time schemes. The choice of τ is a key issue which has been discussed in e.g. Jeuken et al. (1996). If τ is too long, the model will have too much freedom relative to the reference data while when it is too short the above mentioned spinup problems can become severe, depending on the origin of the reference data. Within our experimental set-ups (see below) it was possible to choose small τ values whereby the last fraction in the equation is a good approximation to R because the relaxed simulation stays very close to Ψ^{REF} . It is $R_{n,m}(t)$ estimated this way which is used in the temporal linear regression (5). Note that the assimilation runs (6), have generally been performed without any horizontal diffusion, i.e., $h_n = 0$ for all prognostic variables, since it is the h_n -function we want to estimate.

Our first choice was to estimate R by assimilating dynamical variables (mass and wind fields) from ECMWF re-analysed data (ERA) assimilated at T106 and available every 6 hours into the ARPEGE model at T42 resolution using a τ -value of 6-hours and a cubic spline in time to obtain Ψ^{REF} at intermediate times. Estimated this way R reflects tendency errors from all types of processes not perfectly modelled in ARPEGE relative to the ERA assimilation. The reason for only assimilating the dynamical variables was to let the physical parameterisation work as freely as possible minimising problems related to moisture spinup as in Jeuken et al. (1996). An iterative experimental set-up was used to obtain the final EIFs which had structures qualitatively very similar to those to be shown below. The EIFs were, however, quite different from the EIF obtained by KB. One may thus speculate that KB would have obtained a different result if they used not only the rotational part of the flow in the calculation of their EIF. Another possibility is, however, that we have misinterpreted some of the ARPEGE model deficits relative to analyses (the R -term) as horizontal diffusion. One example could be that vertical diffusion may be too weak in ARPEGE compared to the parameterisation in the analysis assimilation model and that this could lead to large artificial EIF values. Similar potentially unrealistic EIF values could be related to different parameterisation of convection and radiation as well as to errors in the mountain form drag and gravity wave drag parameterisation in ARPEGE at T42 truncation. We do not believe, however, that the relatively long nudging time compared to the typical time scale of waves at T42 and the smoothing related to temporal interpolation constitute serious problems in using

ERA-data. This is because we can re-construct the standard model horizontal diffusion almost exactly in an identical twin experiment (not shown) with similar experimental design as in the case of the analyses.

Since non-linear scale interactions at low wave numbers are well resolved in high resolution models, one may use data from a high resolution version of the low resolution model to be tuned, instead of the analysed data, which to a high degree is generated by a model anyway. But still there will be problems related to orography and furthermore, the physical parameterisation will behave quite differently at the high and low resolution (Williamson, 1999). Therefore, to avoid any misinterpretations in the EIFs, we have chosen to create the reference data in a high resolution adiabatic model configuration and with orography at low resolution. This data set can then be used to estimate EIFs in an equivalent adiabatic version at low horizontal resolution. The following recipe describes the experimental set-up:

Run A:

- High horizontal resolution (T106).
- Mountains at same resolution as in Run B.
- Model prognostic variables determined from the equation

$$\Psi_{n,m}(t + \Delta t) = \Psi_{n,m}(t - \Delta t) + 2\Delta t \left\{ \frac{\partial \Psi_{n,m}}{\partial t} \right\}_{Hdyn} + 2\Delta t \frac{(\{\Psi_{n,m}\}_{clim} - \Psi_{n,m}(t - \Delta t))}{\mathcal{T}} \quad (7)$$

where the term indexed *Hdyn* refers to the dynamical or adiabatic tendency in the model (at high resolution), *clim* to data from the standard model climatology and $\mathcal{T} = 24$ hours. The driving reflected in the last term in (7) is only applied to a few wave numbers: $n = 0, \dots, 10$; $m = 0, 1$ for ARPEGE and $n = 0, \dots, 21$; $m = 0$ for ECHAM4.

- Normal high resolution horizontal diffusion, h_n , which is negligible for the resolved wave numbers of Run B. There is no parameterisation of vertical diffusion.
- Data (reference data set) is obtained by storing at each time step.

Run B:

- Low horizontal resolution (e.g. T21).
- Mountains at same low horizontal resolution (e.g. T21).

- Model prognostic variables determined from an equation similar to (7) but with additional explicit “hard nudging” towards Run A:

$$\Psi_{n,m}(t + \Delta t) = \Psi_{n,m}^{LOW}(t + \Delta t) + 2\Delta t \frac{(\Psi_{n,m}^{HI}(t + \Delta t) - \Psi_{n,m}^{LOW}(t + \Delta t))}{2\Delta t} \quad (8)$$

where *HI* refers to high resolution reference data from Run A and $\Psi_{n,m}^{LOW}(t + \Delta t)$ is a low resolution adiabatic forecast including the simple driving

$$\Psi_{n,m}^{LOW}(t + \Delta t) \equiv \Psi_{n,m}(t - \Delta t) + 2\Delta t \left\{ \frac{\partial \Psi_{n,m}}{\partial t} \right\}_{Ldyn} + 2\Delta t \frac{(\{\Psi_{n,m}\}_{clim} - \Psi_{n,m}(t - \Delta t))}{\mathcal{T}} \quad (9)$$

where the term with index *Ldyn* refers to the dynamical (adiabatic) tendency in the model (at low resolution). Note that the driving is applied to the same wave numbers as in Run A.

- No horizontal diffusion at all ($h_n = 0$). No vertical diffusion.
- Low resolution data (Ψ and Ψ^{LOW}) is obtained by storing at 6 hour intervals.

Note, the “hard nudging” implies that the last fraction in (8) represents the *exact* tendency error, $R_{n,m}(t)$, of Run B relative to Run A since it follows from (8) that $\Psi_{n,m}(t + \Delta t) = \Psi_{n,m}^{HI}(t + \Delta t)$, i.e., the values in the low resolution model are continually reset to the reference values at the end of each integration step. Then $\Psi_{n,m}(t - \Delta t) = \Psi_{n,m}^{HI}(t - \Delta t)$ whereby it is easily seen from (7), (8) and (9) that R is the difference or error in the low resolution full dynamical tendency relative to the high resolution tendency:

$$R_{n,m}(t) = \left\{ \frac{\partial \Psi_{n,m}}{\partial t} \right\}_{Hdyn} - \left\{ \frac{\partial \Psi_{n,m}}{\partial t} \right\}_{Ldyn} \quad (10)$$

By our experimental set-up it is ensured that the tendency error can *only* be due to unresolved dynamical scale interactions. As an example from the vorticity equation, all unresolved scale interactions associated with the terms

$$-\mathbf{V} \cdot \nabla \eta - w \frac{\partial \eta}{\partial z} - \eta \delta + \mathbf{k} \cdot \nabla w \times \frac{\partial \mathbf{V}}{\partial z} + \mathbf{k} \cdot \nabla p \times \nabla \alpha \quad (11)$$

contribute to R (here in geometric height co-ordinates for simplicity). In (11) \mathbf{V} is the full wind field, η the absolute vorticity, w the vertical velocity, δ the divergence, \mathbf{k} a unit vertical vector, p the pressure and α the specific volume.

The exact adiabatic tendency errors relative to model versions truncated at T106 have been used to obtain EIFs for ARPEGE truncated at T21, T30 and T42 and for ECHAM4 at T30. Referring to Table 1 which lists all the needed simulations, Run 2 and Run 3, respectively, are Run A and Run B type simulations. Similarly, Run 5/Run 6, Run 8/Run 9, Run 14/Run 18, Run 15/Run 19, Run 16/Run 20, Run 17/Run 18 are pairwise of Run A and Run B types. Run 1, 4, 7, 10, 11, 12 and 13 are used to generate the climatology for driving the adiabatic simulations. The objectives behind this rather comprehensive choice of experiments are that we want to investigate how the derived EIFs depend on the resolution and on the season, and hence on the characteristics of the large-scale mean flow.

4. EIFs obtained from exact adiabatic tendency errors.

In this section the EIFs obtained from the exact adiabatic tendency errors are presented. As an important first example Fig. 3 shows the raw EIF ($\hat{h}_{n,m}$), depending on both total (n) and zonal (m) wave number, for vorticity at level 14 (approximately 360 hPa) in ARPEGE/T21, estimated from tendency errors in Run 3 relative to Run 2 (see Table 1). Generally this $\hat{h}_{n,m}$ appears somewhat noisy but clearly shows small negative values for low and intermediate total wave numbers and positive values for high wave numbers. This means that non-linear interactions with unresolved scales lead to an amplification of vorticity at low to intermediate wave numbers and a damping at high wave numbers. It is interesting that the $\hat{h}_{n,m}$ in Fig. 3 has a systematic variation not only with n but also with m . One may therefore suspect that a parameterisation of the same form as in (4) but involving also a zonal wave number dependency in the EIFs might give more realistic results than the values \hat{h}_n (averaged over m) which have been used here. The variation with zonal wave number is generally strongest for vorticity but is also seen for divergence and temperature (not shown). Using $\hat{h}_{n,m}$ with negative values for both n and m close to the truncation limit will be investigated further in a subsequent paper.

The vertically varying EIFs (\hat{h}_n) for vorticity, divergence and temperature depending on total wave number only are shown in Fig. 4 for ARPEGE/T21. For high wave numbers the EIFs generally become positive with e-folding times close to one day at the truncation limit ($n=21$). An interesting feature which we cannot explain is the negative EIF values for temperature at the truncation limit around model level 20. One

may suspect that this represents a flaw in our approach. We have therefore tested several possibilities ranging from estimating tendency errors via “soft” nudging (6) with different values of τ , omitting the time-filtering in the simulations, and performing the simulation with explicit instead of semi-implicit time stepping schemes. None of these tests gave results different from Fig. 4. The EIF for divergence stays positive for all total wave numbers and increases less steeply near the truncation limit than the two other EIFs. The most important feature of Fig. 4 is, however, that the negative EIF values in Fig. 3 are not only confined to level 14 but are seen both for vorticity and temperature in large parts of the atmosphere approximately between total wave numbers 5 and 15. The concept of a negative diffusion at intermediate wave numbers is consistent with the results of Leith (1971) and KB. Leith (1971) calculated a spectral diffusion function for two dimensional turbulence assuming the model was truncated at a wave number located in an enstrophy cascading inertial subrange, while KB obtained their EIF without this assumption. The main difference between KB's EIF and ours is that we obtain no maximum damping at the jet level for higher wave numbers, but rather a vertically more constant damping with a maximum near the lower boundary. Furthermore, as mentioned above we obtain rather different damping for the different prognostic variables, whereas KB calculated an EIF for vorticity only. The differences between KB's EIF and our EIF for the vorticity equation is mainly due to our inclusion of all dynamical processes on the right hand side of the equation (see (11)). When the effects associated with the term $-\mathbf{V}\cdot\nabla\eta$, where \mathbf{V} includes the divergent wind component are examined using the same methodology as in KB, an EIF similar to Fig. 4a is obtained (J.N. Koshyk, private communication). When the term $-\eta\delta$ is included, an EIF very similar to the one in KB is obtained. The implication is that there is a considerable cancellation between the effect from the terms $-\eta\delta$ and $-\mathbf{V}_d\cdot\nabla\eta$, where \mathbf{V}_d is the divergent wind component. One can say our work is a further extension including also vertical advection, tilting and solenoidal terms for the vorticity equation and that these are the terms mainly responsible for the differences from KB's results. It should, however, be kept in mind that divergence and vertical velocity are closely related in an approximate hydrostatic atmosphere. This means that for typical atmospheric circulation systems *all* the terms $-\eta\delta$, $-\mathbf{V}_d\cdot\nabla\eta$, $-w\partial\eta/\partial z$ and $\mathbf{k}\cdot\nabla w\times\partial\mathbf{V}/\partial z$ are linked and to a high degree cancel each other, implying that it is hard to say which single term is responsible for the differences between KB's EIF and ours. It should be noted that the differences in the EIFs are probably not due to our

regression methodology (5) since we as expected have obtained essentially the same EIF as in Fig. 4a (but slightly more noisy) from

$$\hat{h}_n(t) = \frac{\frac{1}{2\Delta t} \left(\overline{\sum_{m=-n}^n |\zeta_{m,n}^{LOW}|^2} - \overline{\sum_{m=-n}^n |\zeta_{m,n}|^2} \right)}{2 \overline{\sum_{m=-n}^n |\zeta_{n,m}|^2}} = \frac{\overline{\left(\frac{E_n^{LOW} - E_n}{2\Delta t} \right)}}{2\overline{E_n}} = \frac{-\overline{K_n^U}}{2\overline{E_n}} \quad (12)$$

where ζ is relative vorticity, E_n the rotational part of the kinetic energy for total wave number n , K_n^U the non-linear interactions from all unresolved adiabatic processes and the overbars denote temporal averaging. Equation (12) is quite similar to the energy interaction equation (15) in KB – the only important difference is that the unresolved rotational advective scale interactions in the nominator of KB’s equation are replaced by K_n^U .

The structures of the EIFs (not shown) for ARPEGE/T30 and ARPEGE/T42 are very similar to those in Fig. 4, however with higher positive values near the truncation limit and with smaller negative values at the intermediate wave numbers. In the T42 case all positive values are approximately doubled relative to Fig. 4 and the negative almost halved. For T42 the negative EIF values for vorticity are generally seen at total wave numbers between 10 and 30.

Fig. 5 is equivalent to Fig. 4, but for ECHAM4/T30, and based on tendency errors of Runs 18-21, relative to Runs 14-17. Taking into account that the two models have a different distribution of vertical levels the figures are quite similar except near the top of the model, where strong positive values are found in ECHAM4. These positive values are no more than re-constructions of the original T106 damping (in Runs 14-17) near the top of the model which is introduced to avoid spurious wave reflection at the top of the model atmosphere.

The EIFs in Fig. 4 and 5 are characterised by considerably lower values than the standard spectral damping function (h_n) in the two models which is positive for all wave numbers. The differences are largest for ARPEGE, but are also considerable for ECHAM4.

A question which naturally arises is how stable the results are - or in other words if they depend on the actual flow in the adiabatic simulations (Run A and Run B type simulations). This has been tested for winter data in the ARPEGE by considering

the 4 individual 30 days of Run A and Run B type simulations (making up Run 2 and Run 3) which were started from initial conditions in 4 different winters. In spite of the simple adiabatic approach the flow in the 4 simulations is rather dissimilar, but the EIFs (not shown) are all very similar to those in Fig. 4. A possible variation with season has also been investigated. This was done by calculating individual EIFs for Jan., Apr., Jul., and Oct. in ECHAM4/T30 (see Table 1). These EIFs (not shown) were all very similar to those in Fig. 5, albeit somewhat noisier. For ARPEGE, the results were further investigated by taking only the first 10 days of each adiabatic simulation into account. This may be relevant, since the simulated flow in the beginning of the simulations is least affected by the simple zonal mean driving and the fact that the models are run adiabatically. But also in this case no noteworthy differences were seen from Fig. 4 and we therefore conclude that the EIFs are very stable and constitute fundamental features of the (model) atmospheres.

The tendency errors of Run B relative to Run A type simulations can be used to calculate the unresolved kinetic energy dissipation, i.e., the dissipation due to interactions with unresolved scales, taking all dynamical interactions into account and not only those involving the rotational part of the flow (as in KB). Fig. 6a shows the exact long term and zonal mean kinetic energy generation resulting from unresolved scale interactions in Run 3 relative to Run 2. The dissipation was simply calculated from total kinetic energy in grid point space before and after nudging. Regions of strong kinetic energy generation and dissipation are seen near the jet streams, a picture which is most clear in the SH and more chaotic in the Northern Hemisphere (NH), where the quasi-stationary eddies are stronger. Considerable dissipation is also seen near the planetary boundary layer, while weak dissipation dominates over the rest of the atmosphere. It should be mentioned that the specific location of the positive and negative values depends on the mean flow in the adiabatic runs. The jet-stream locations in these simulations are, however, similar to those in the observed climate.

Fig. 6b is obtained in the same way as Fig. 6a by replacing the values of vorticity and divergence after nudging by the values before nudging plus the right hand side of (5) times $2\Delta t$. This shows how well the unresolved dissipation in Fig. 6a is parameterised. The amplitudes in Fig. 6b are generally much smaller than in Fig. 6a except for the boundary layer, where they are comparable. Furthermore, the position of the regions of energy generation are not well aligned with those in Fig. 6a. Fig. 6b raises

serious doubts that a formulation of the form (4) adequately can parameterise the effect of unresolved scale interactions for models at low truncation. If the EIFs in Fig. 4 are replaced by the original h_n -function in ARPEGE, the situation is even worse since this function is positive definite, and therefore the corresponding HD is purely diffusive as illustrated in Fig. 6c. Fig. 6d is equivalent to Fig. 6a, but is based on T30 model truncation, i.e., Runs 5 and 6. At this resolution the truncation errors are smaller, leading to weaker and less systematic patterns of unresolved generation/dissipation of kinetic energy. This is probably the main reason that improved model performance relative to T21 usually is seen at resolution T30 and higher. When inserting the EIFs for T30 (not shown) it can further be seen, that also at this resolution the effect of unresolved scale interactions calls for an improved type of parameterisation (Fig. 6e). Fig. 6f is for resolution T42, i.e., based on Run 8 and 9. One might be tempted to consider Fig. 6f as a justification of the use of T42 as truncation in many climate models around the world since the statistical effect of unresolved scales relative to T106 is much smaller than at T30 in the free atmosphere. Obviously, this statement relies on the assumption that no or little additional dissipation error would be seen if the reference run (Run 8 in Table 1) was performed at much higher resolution than T106. We have not yet tested if this is the case, and therefore, cannot conclude from our present experiments that T42 should be a kind of optimal choice of truncation for climate simulations. The parameterisation of the unresolved dissipation in Fig. 6f is shown in Fig. 6g which is based on the T42 EIFs (not shown). The positive values in parts of the NH (Fig. 6f) are not well parameterised. It should, however, be noted that Run 8 and 9 only cover 30 days each and that a smoother pattern with less positive areas than in Fig. 6f probably would be seen in case of longer simulations.

KB presented plots of the parameterised effect of unresolved scales for a T32 truncation (their Fig. 7a) which are derived in the same way as our Fig. 6b, 6e, and 6g. As expected, our EIFs lead to higher diffusion in the lower part of the atmosphere but otherwise the plots have many features in common.

5. Long perpetual January simulations.

A GCM employing horizontal diffusion tends to readjust to counteract the effect of the diffusion. This is mainly because the wind and mass fields are brought out of their mutual balance by the diffusion term and consequently the model tends to re-establish the balance via geostrophic adjustment. Therefore it is interesting to investigate

how the two GCMs behave when the EIFs are used in long (free) simulations, i.e., with h_n set to the EIF values in Fig. 4 and 5. This investigation was in our case done by comparing perpetual January simulations using the original and the new h_n -values and further comparing these with simulations performed at higher spatial resolution.

For ARPEGE/T21 two simulations, referred to as Run 24 and 25 in Table 1, were integrated for 1000 days with full physical parameterisation. Run 24 serves as a control and is performed with the original model diffusion, while Run 25 is run with h_n set to the EIF values in Fig. 4. Run 26 serves as the high resolution model "truth" and is performed with full physics at a horizontal resolution of T42 and with standard T42 horizontal diffusion which is negligible at total wave number 21. Fig. 7a shows the long term difference in MSLP between the last 850 days of Run 26 and Run 24, and Fig. 7b the difference between the last 850 days of Run 25 and Run 24. First, it should be noted that over the SH there is a very high degree of similarity between Fig. 7a and Fig. 1 (based on Run 23 and 10 with ECHAM4) with considerably deeper pressure over Antarctica and much stronger zonal winds around 60°S in the high resolution simulations. Also the resolution dependent differences in the SH eddies are very similar. Over the NH, there are essentially no common features, which may partly be due to the sampling periods (600 days in Fig. 1 and 850 in Fig. 7) which, in view of the large degree of low-frequency variability there, are too short to obtain statistically robust differences. Furthermore, the orography is different in Run 26 and 24, while it is the same in Run 23 and 10. The impact of using the EIFs is seen in Fig 6b and it is noted that there are some similarities with Fig. 7a in the SH with a deepening of the pressure near Antarctica. In the NH, however, Fig. 7a and Fig. 7b are almost opposite and the new EIFs lead to less realistic MSLP patterns than the original HD, when compared to Run 26 or to analyses (not shown).

For ECHAM4/T30 the control simulation is identified as Run 10 in Table 1 while Run 22 is the corresponding simulation with h_n replaced by the EIFs in Fig. 5 and Run 23 is the model "truth" which in this case is a T106 simulation with all orographic processes (i.e., mean orography and parameters for the gravity wave drag scheme) behaving as in the T30 version. Run 10, 22 and 23 were all integrated for 750 days with full physics. Fig. 8 shows the long term difference between the last 600 days of Run 22 and Run 10. It is seen that the patterns of differences in Fig. 1 and Fig. 8 are quite similar, particularly over the SH. Thus the re-tuned model behaves somewhat more like a

higher resolution model version than the original model - a result which is much better than for ARPEGE/T21. Over the NH, however, the variability is generally too large to obtain significant difference maps - except over eastern Siberia, where the sign in both Fig. 8 and Fig. 1 is negative. While the patterns in Fig. 8 and Fig. 1 are similar the amplitude in Fig. 8 is too small to make the T30 model climate equal to that of the T106 model. One may anticipate that this is partly due to readjustments as mentioned above, and partly due to the simple form (4) of the parameterisation.

The spectrum of kinetic energy at 500 hPa in Run 24, 25 and in ERA January (1982, 85, 88 and 91) data is shown in Fig. 9. There are considerable differences for low wave numbers which may be due to severely truncated orography in ARPEGE/T21 as well as to inadequate parameterisation (including HD). For high total wave numbers the ERA data follows the -3 power law closely, and Run 25 is generally closer to the ERA data, than Run 24. There are, however, some signs of so-called spectral blocking, i.e., a concentration of energy near the truncation limit, in Run 25. For ECHAM4/T30 which is plotted in Fig. 10 there are no signs of spectral blocking, but otherwise the picture is largely the same as for ARPEGE. It is likely that the tendency for spectral blocking in ARPEGE/T21 could be related to the readjustments.

6. Summary and discussion.

We have used tendency errors to obtain empirical interaction functions (EIFs) to be used in the formulation of horizontal diffusion (HD) in two GCMs: ARPEGE (climate version 2) and ECHAM4. In both cases the tendency errors were calculated in an adiabatic low resolution model version relative to a high resolution adiabatic version of the same model. This special experimental design was used to avoid EIF values partly reflecting a different behaviour of physical parameterisation at different horizontal resolution. The EIFs were calculated for three different resolutions, T21, T30 and T42 in ARPEGE, and for T30 in ECHAM4. For all resolutions different EIFs were calculated for the prognostic model variables vorticity, divergence and temperature. At all resolutions and for both models the EIFs for vorticity and to some extent for temperature show negative values at intermediate wave numbers implying that the amplitudes of the waves at these scales are enhanced, i.e., a kind of negative diffusion. The EIFs identified for different seasons and different January flows are all very similar. It is shown that the kinetic energy generation/dissipation due to unresolved non-linear scale interactions varies strongly with model resolution and that it is not well parameterised at T21 and

partly at T30 using the standard formulation of HD in spectral models, i.e., wave amplitude damping. The situation is somewhat - but not satisfactorily - improved if wave amplitude amplification, as given by the negative intermediate wave number EIFs, is permitted. At T42 the truncation errors relative to T106 seem, however, to be much smaller and parameterisable. In a long perpetual January GCM simulation with ECHAM4 truncated at T30, the pattern of mean sea level pressure, particularly over the SH, was in better agreement with a high (T106) resolution simulation when using the EIFs instead of the purely diffusive standard horizontal diffusion in ECHAM4. The most interesting feature is probably that the pressure gradient between subtropical and subarctic regions in the SH is considerably increased using the new EIFs. A simulation with ARPEGE truncated at T21 did not show similar improvement supporting the idea that an entirely revised formulation of HD is needed for low resolution models. The spectrum of kinetic energy in the middle troposphere is generally in better agreement with observations when EIFs are used instead of standard model HD, even though there are weak signs of so-called spectral blocking.

Because of the dramatic growth in performance of computers the present work is mainly of interest in connection with very long low to medium resolution coupled GCM simulations aiming at palaeo-climate or coupled atmosphere-ocean studies. In such simulations - as in climate sensitivity studies - it is important that systematic errors in the atmospheric GCM are small. Otherwise severe flux corrections (e.g. Cubasch, 1989) are needed for the ocean GCM to avoid unrealistic climate drift of the coupled model. As an example, it is obvious from the preliminary investigation of our perpetual January simulations that e.g. the near surface zonal flow (and therefore the turbulent fluxes) around Antarctica is very sensitive to resolution and to the formulation of HD (Fig. 1, 7 and 8). Even though not investigated in the present paper, one may further anticipate that an improved HD will also lead to better simulation of low-frequency phenomena in the atmosphere like blocking of the westerlies, since strong non-linear interactions are important in forming and maintaining these phenomena (see e.g. Nakamura et al., 1997; Holopainen and Fortelius, 1987)

A main conclusion of the present work is that a new type of parameterisation of non-linear dynamic scale interactions is needed for low resolution GCMs to replace the standard formulation in (4), since this formulation can not ensure realistic dissipation/generation of kinetic energy (Fig. 6). It is believed that our method based on

minimisation of tendency errors in a low resolution model relative to a high resolution version of the same model is a powerful tool not only to identify EIFs for the formulation in (4), but also for developing and tuning a new parameterisation. One may argue that an adiabatic model version as we have used is too unrealistic for this purpose. It is, however, relatively easy to generalise the experimental design described in section 3 in such a way that the driving in Run A and Run B is by identical diabatic forcing. This will only require an extra T106 simulation and storing of truncated diabatic tendencies each time step.

A simple potential improvement to the formulation (4), to be investigated in a subsequent paper will be to let the EIFs vary with zonal as well as total wave number. More advanced parameterisations like the anticipated potential vorticity method by Sadourny and Basdevant (1985) may also be used as inspiration for developing new algorithms. Since the nature of vertical advection generally changes between high and low resolution, some part of the tendency errors, particularly in the planetary boundary layer, might be parameterised more efficiently via vertical diffusion than via the horizontal parameterisation in (4).

It is noted that the technique outlined in this paper is well suited for optimising parameterisation of unresolved dynamical scale interactions in models employing an adiabatic formulation different from ARPEGE/IFS and ECHAM4. In spectral models employing semi-Lagrangian advection schemes the handling of non-linear interactions is done via the interpolations at the trajectory departure points. There is, however, no formal control over the cascades of energy and enstrophy in these models, and it is therefore anticipated that the diffusion also in such models could be optimised successfully by minimising tendency errors. It is also important to point out that the HD in grid point models, Eulerian or semi-Lagrangian, can be formulated and/or tuned using techniques equivalent to those presented here.

7. Acknowledgements

We thank John Koshyk (University of Toronto); Leif Laursen (DMI); and Bennert Machenhauer, Erich Roeckner and Lennart Bengtsson (Max-Planck-Institute for Meteorology) for fruitful discussions. The work was financially supported by the European Commission's 4th FRAMEWORK PROGRAMME, "Environment and Climate Research Programme" under contract number ENV4-CT95-0101 ("MILLENNIA") and by the Nordic Council of Ministers under contract no. FS/HFj/X-93002 ("NOCLIMP").

References

- Boer, G. J. and T. G. Shepherd, 1983. Large-scale two-dimensional turbulence in the atmosphere. *J. Atmos. Sci.*, **40**, 164-184.
- Boville, B. A., 1991. Sensitivity of simulated climate to model resolution. *J. Clim.*, **4**, 469-485.
- Boyle, J. S., 1993. Sensitivity of dynamical quantities to horizontal resolution for a climate simulation using the ECMWF (cycle 33) model. *J. Clim.*, **6**, 796-815.
- Cubasch, U., 1989: Coupling a global atmosphere model with a global ocean model using the flux correction method. In "*Aspects of coupling atmosphere and ocean models*", Rep. No. **6.**, Met. Inst. Univ. Hamburg, Germany.
- Déqué, M. and J. P. Piedelievre, 1995: High resolution climate simulation over Europe. *Clim. Dyn.* **11**, 321-339.
- Déqué, M., C. Drevet, A. Braun, D. Cariolle, 1994. The ARPEGE/IFS atmosphere model: a contribution to the French community climate modelling. *Clim. Dyn.*, **10**, 249-266.
- Holopainen, E. O., and C. Fortelius, 1987: High-frequency transient eddies and blocking. *J. Atmos. Sci.*, **44**, 1632-1645.
- Jeuken, A.B.M., P.C. Siegmund, L.C. Heijboer, J. Feichter and L. Bengtsson, 1996. On the potential of assimilating meteorological analyses in a global climate model for the purpose of model validation. *J. Geophys. Res.*, **101**, 16939-16950.
- Koshyk, J.N. and G.J. Boer, 1995. Parameterisation of dynamical subgrid-scale processes in a spectral GCM, *J. Atmos. Sci.*, **52**, 965-976.
- Kraichnan, R. H., 1967. Inertial ranges in two-dimensional turbulence. *Phys. Fluids*, **10**, 1417-1423.
- Laursen, L. and E. Eliassen, 1989. On the effects of the damping mechanisms in an atmospheric general circulation model. *Tellus*, **41A**, 385-400.
- Leith, C. E., 1968. Diffusion approximation for two-dimensional turbulence. *Phys. Fluids*, **11**, 671-673.
- Leith, C. E., 1971. Atmospheric predictability and two-dimensional turbulence. *J. Atmos. Sci.*, **28**, 145-161.
- Nakamura, H., M. Nakamura, and J. L. Anderson, 1997: The role of high and low frequency dynamics in blocking formation, *Mon. Wea. Rev.*, **125**, 2074-2093.

- Roeckner, E., K. Arpe, L. Bengtsson, M. Christoph, M. Claussen, L. Dümenil, M. Esch, M. Giogette, U. Schlese and U. Schulzweida, 1996: The atmospheric general circulation model ECHAM-4: Model description and simulation of present-day climate. *Max-Planck-Institute für Meteorologie*, Report No. **218**, 90pp.
- Sadourny, R. and C. Basdevant, 1985: Parameterization of subgrid scale barotropic and baroclinic eddies in quasi-geostrophic models: Anticipated Potential Vorticity Method. *J. Atmos. Sci.*, **42**, 1353-1363.
- Stendel, M. and E. Roeckner, 1998. Impacts of horizontal resolution on simulated climate statistics in ECHAM4. *Max-Planck-Institute für Meteorologie*, Report No. **253**, 57 pp.
- Wiin-Nielsen, A., 1967. On the annual variation and spectral distribution of atmospheric energy. *Tellus*, **19**, 540-559.
- Williamson, D. L., 1999: "Convergence of atmospheric simulations with increasing horizontal resolution when the scale of parameterization is held fixed". *Tellus, Special Issue*, in press.

Run	Model	Hor. Res.	Vert. Res.	Orog.	Diff.	Driving	Solar forcing	Ref.	Lenght
1	ARPEGE	T106	L31	T21	original	Physics	Annual Cyc. (Jan)	-	30 days
2	ARPEGE	T106	L31	T21	original	Run 1	-	-	120 days ^b
3	ARPEGE	T21	L31	T21	none	Run 1	-	Run 2	120 days ^b
4	ARPEGE	T106	L31	T30	original	Physics	Annual Cyc. (Jan)	-	30 days
5	ARPEGE	T106	L31	T30	original	Run 4	-	-	30 days
6	ARPEGE	T30	L31	T30	none	Run 4	-	Run 5	30 days
7	ARPEGE	T106	L31	T42	original	Physics	Annual Cyc. (Jan)	-	30 days
8	ARPEGE	T106	L31	T42	original	Run 7	-	-	30 days
9	ARPEGE	T42	L31	T42	none	Run 7	-	Run 8	30 days
10	ECHAM4	T30	L19	T30	original	Physics	Perp. Jan.	-	750 days
11	ECHAM4	T30	L19	T30	original	Physics	Perp. Apr.	-	30 days
12	ECHAM4	T30	L19	T30	original	Physics	Perp. Jul.	-	30 days
13	ECHAM4	T30	L19	T30	original	Physics	Perp. Oct.	-	30 days
14	ECHAM4	T106	L19	T30	original	Run 10	-	-	30 days
15	ECHAM4	T106	L19	T30	original	Run 11	-	-	30 days
16	ECHAM4	T106	L19	T30	original	Run 12	-	-	30 days
17	ECHAM4	T106	L19	T30	original	Run 13	-	-	30 days
18	ECHAM4	T30	L19	T30	none	Run 10	-	Run 14	30 days
19	ECHAM4	T30	L19	T30	none	Run 11	-	Run 15	30 days
20	ECHAM4	T30	L19	T30	none	Run 12	-	Run 16	30 days
21	ECHAM4	T30	L19	T30	none	Run 13	-	Run 17	30 days
22	ECHAM4	T30	L19	T30	new	Physics	Perp. Jan.	-	750 days
23	ECHAM4	T106	L19	T30	original	Physics	Perp. Jan.	-	750 days
24	ARPEGE	T21	L31	T21	original	Physics	Perp. Jan.	-	1000 days
25	ARPEGE	T21	L31	T21	new ^c	Physics	Perp. Jan.	-	1000 days
26	ARPEGE	T42	L31	T42	original	Physics	Perp. Jan.	-	1000 days

Tables

Table 1. List of the GCM-simulations used in the present paper. Columns indicate: 1) Simulation number; 2) Model; 3) Spectral truncation of prognostic variables (horizontal); 4) Number of vertical levels; 5) Spectral truncation of orography used; 6) Spectral damping (horizontal diffusion) with "original" indicating the damping in the standard version of the model for that particular horizontal truncation, "new" the empirically derived damping, and "none" no damping of any wave components; 7) Driving of

^b In reality Run 2 and Run 3 are merges of four 30 day simulations with identical driving (weak relaxation towards Run 1) but started from analysed initial conditions on the 1 January in 1982, 1985, 1988 and 1991.

^c Based on Run 3.

simulation with "Physics" indicating the standard physical parameterisation of the model at its given horizontal resolution, and "Run #" indicating the data set towards which the actual simulation is being weakly relaxed in its zonal mean and zonal wave number 1 (see text); 8) Type of solar forcing (annual solar cycle or perpetual forcing) in case of "Physics" in column 7); 9) Reference data set towards which the actual simulation is being nudged for all dynamical variables. This data set is stored each time step; 10) Length of simulation.

FIGURE CAPTIONS

- Fig. 1. Long term difference in mean sea level pressure (MSLP) between the 600 last days of two perpetual January simulations at T106 and T30 horizontal resolutions made with the ECHAM4 model. Orography is truncated to T30 in both simulations. Contour interval: 2 hPa with negative contours dashed.
- Fig. 2. Vertical distribution of the σ - p hybrid (half) levels in ECHAM4 (panel a) and ARPEGE/IFS (panel b). Left vertical axis shows pressure, while the right axis shows the half level number.
- Fig. 3. EIF depending on zonal wave number ($\hat{h}_{m,n}$) obtained from Run 2 and Run 3 (see Table 1) at model level 14 for vorticity. Vertical axis shows total wave number and horizontal axis shows zonal wave number, m . Units are day^{-1} with contours at -.2, -.1, -.05, -.02, -.01, 0., .01, .02, .05, .1, .2, .5, 1., 2., 5., with positive values shaded and negative stippled.
- Fig. 4. Empirical interaction function (\hat{h}_n) for vorticity (a), divergence (b) and temperature (c) in the T21 version of ARPEGE calculated from tendency errors of Run 3 relative to Run 2. Vertical axis shows model level with level 1 at top of model. Horizontal axis shows total wave number, n . Units and contouring are as in Fig. 3.
- Fig. 5. As Fig. 4, but for ECHAM4 at T30 resolution and based on pairwise tendency errors of Runs 18-21 relative to Runs 14-17.
- Fig. 6. Zonal and temporal average of generation of kinetic energy in ARPEGE/IFS due to unresolved scale interactions obtained a) from the tendency errors of Run 3 relative to Run 2, b) from the parameterised interaction term ($-\hat{h}_n \Psi_{n,m}(t)$) using the data from Run 2 and the T21 EIFs as in Fig. 4, c) from the standard T21-HF term ($-h_n \Psi_{n,m}(t)$) using the data from Run 2, d) from the tendency errors of Run 6 relative to Run 5, e) from the parameterised interaction term ($-\hat{h}_n \Psi_{n,m}(t)$) using the data from Run 5 and T30 EIFs f) from the tendency errors of Run 9 relative to Run 8, and g) from the parameterised interaction term ($-\hat{h}_n \Psi_{n,m}(t)$) using the data from Run 8 and T42 EIFs. Contour intervals at -70, -60, ..., -20, -15, -10, -5, 0, 5, 10, 15, 20, 30, ..., 70 $\text{m}^2 \text{s}^{-2} \text{day}^{-1}$.
- Fig. 7. Long term difference in mean sea level pressure between a) Run 26 (ARPEGE/T42) and Run 24 (ARPEGE/T21, original diffusion), and b) Run 25 (ARPEGE/T21, new diffusion) and Run 24 (ARPEGE/T21, original diffusion). Contour interval = 2 hPa.

-
- Fig. 8. Long term difference in mean sea level pressure between Run 22 (ECHAM4/T30, new diffusion) and Run 10 (ECHAM4/T30, original diffusion). Contour interval = 1 hPa. (note that the contour interval in Fig. 1 is 2 hPa).
- Fig. 9. Long term average of spectral density of kinetic energy at 500 hPa as function of total wave number (n) for ARPEGE/T21 control simulation (Run 24), stippled; for ARPEGE/T21 new diffusion (Run 25), dashed; and for ERA data in January full line.
- Fig. 10. As Fig. 9, but for ECHAM4/T30 control simulation (Run 10), stippled; and for ECHAM4/T30 new diffusion (Run 22), full line. At the end of each spectrum lines indicating the n^{-3} power law are shown.

Figures

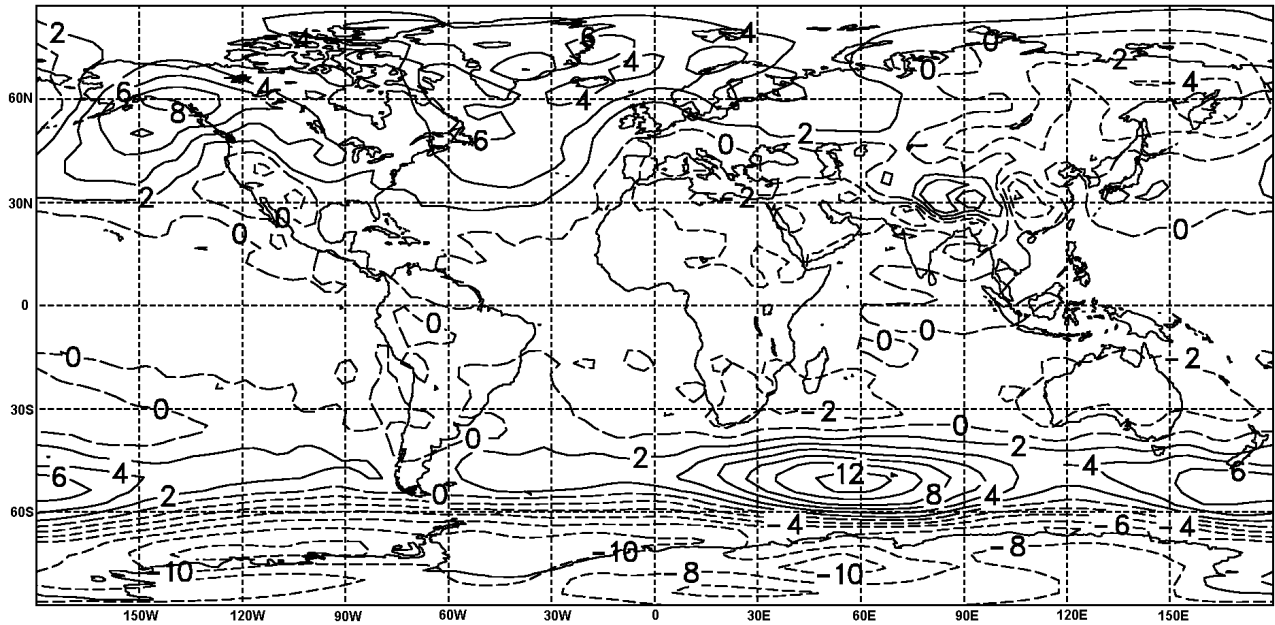


Fig. 1. Long term difference in mean sea level pressure (MSLP) between the 600 last days of two perpetual January simulations at T106 and T30 horizontal resolutions made with the ECHAM4 model. Orography is truncated to T30 in both simulations. Contour interval: 2 hPa with negative contours dashed.

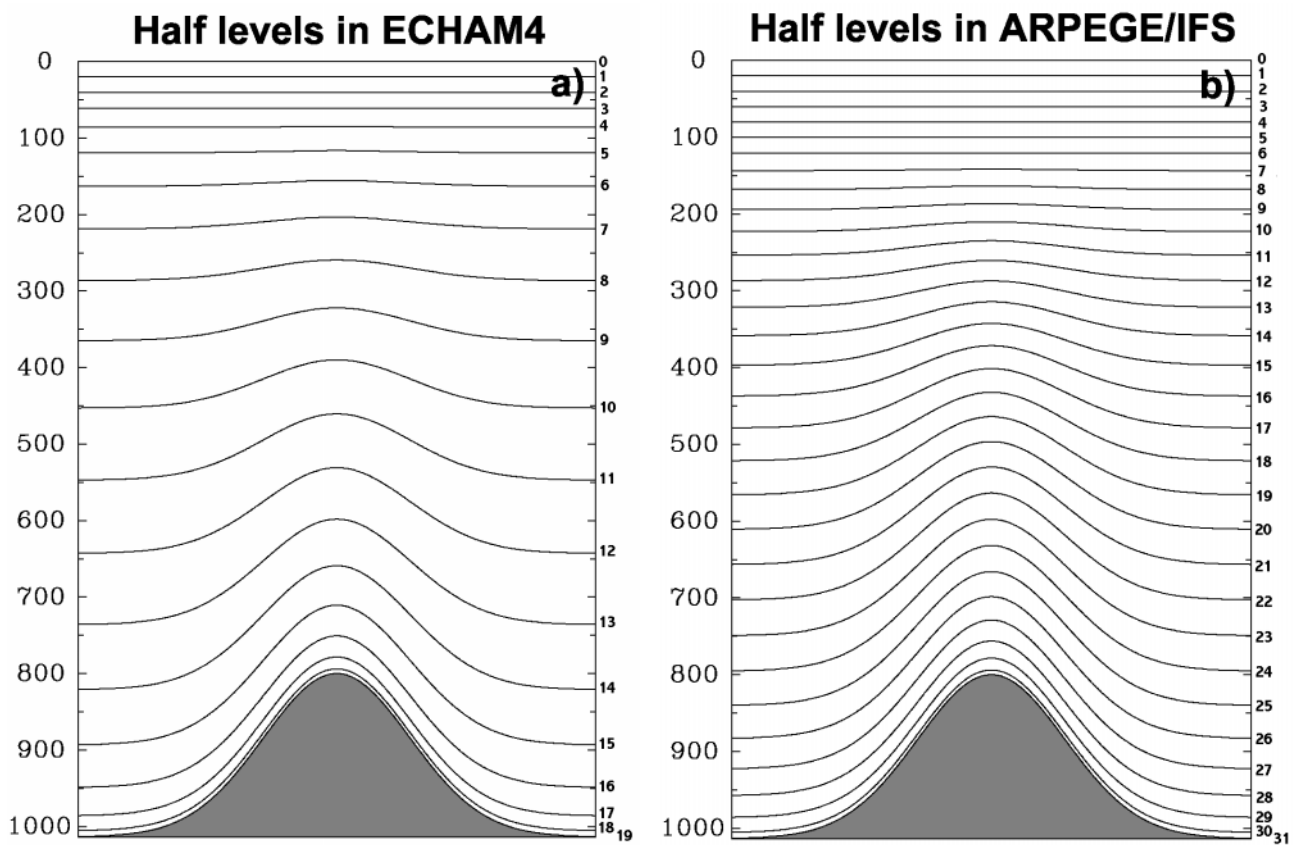


Fig. 2. Vertical distribution of the σ - p hybrid (half) levels in ECHAM4 (panel a) and ARPEGE/IFS (panel b). Left vertical axis shows pressure, while the right axis shows the half level number.

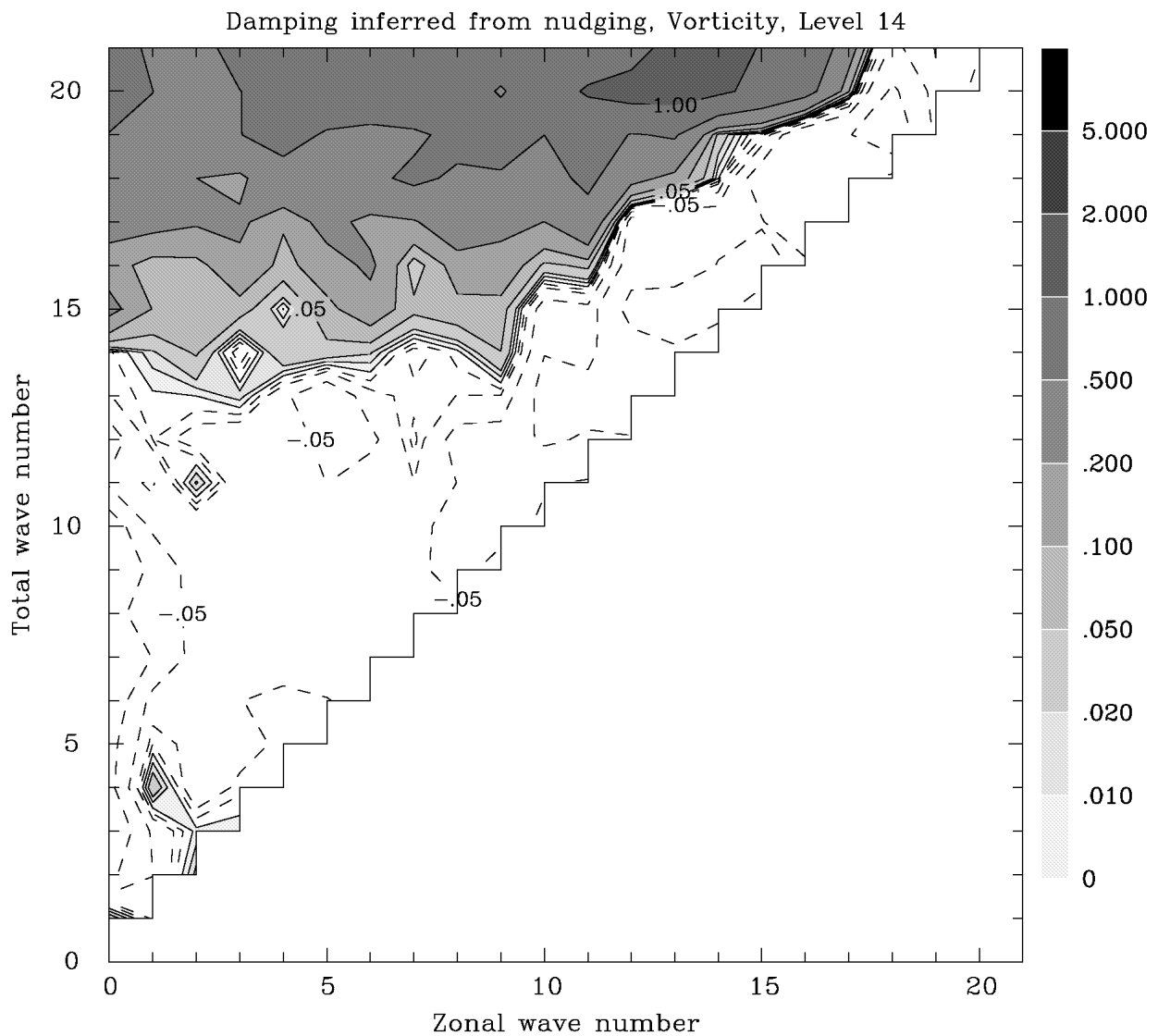


Fig. 3. EIF depending on zonal wave number ($\hat{h}_{m,n}$) obtained from Run 2 and Run 3 (see Table 1) at model level 14 for vorticity. Vertical axis shows total wave number and horizontal axis shows zonal wave number, m . Units are day^{-1} with contours at $-2, -1, -0.5, -0.2, -0.1, 0, .01, .02, .05, .1, .2, .5, 1, 2, 5$, with positive values shaded and negative stippled.

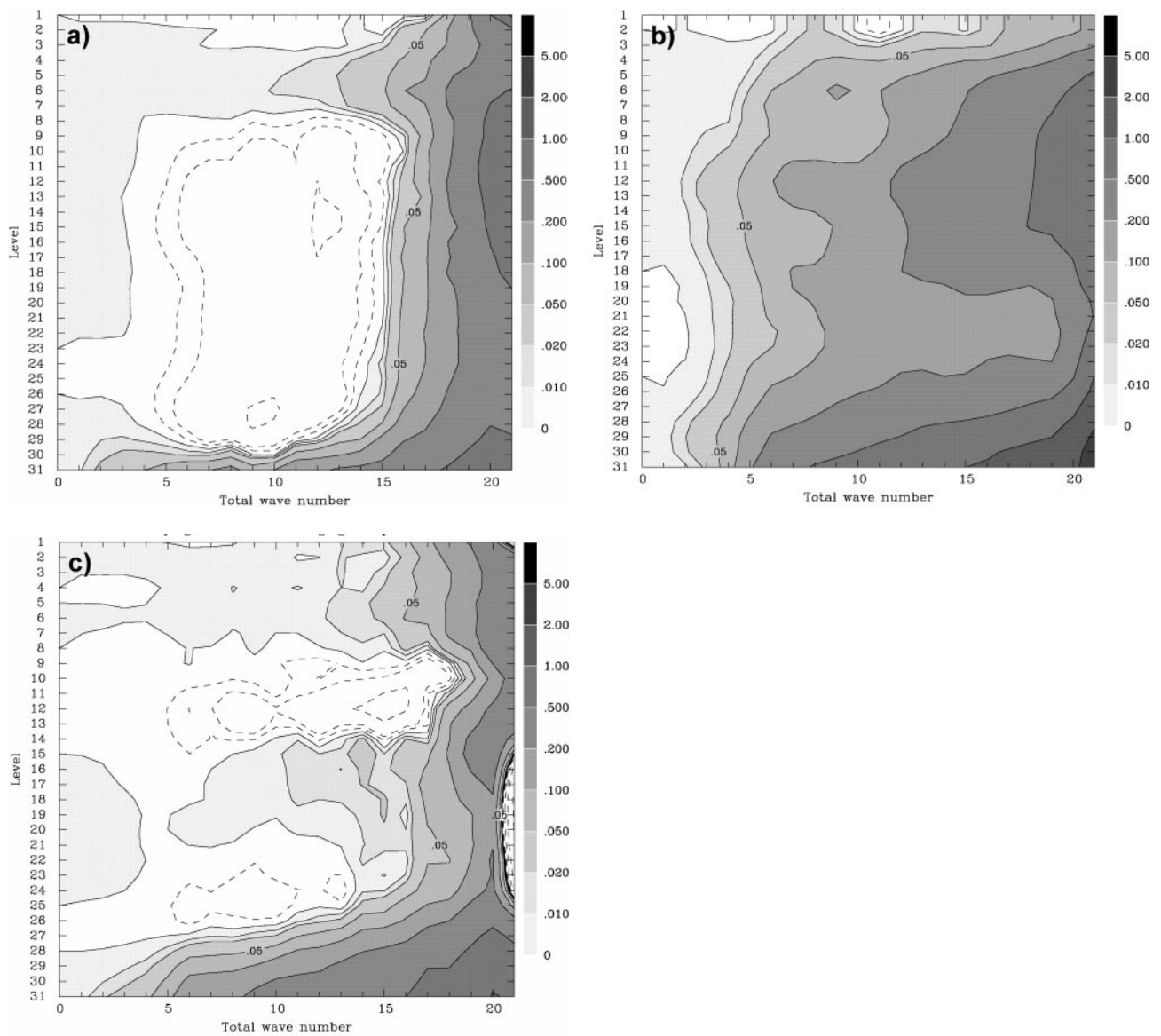


Fig. 4. Empirical interaction function (\hat{h}_n) for vorticity (a), divergence (b) and temperature (c) in the T21 version of ARPEGE calculated from tendency errors of Run 3 relative to Run 2. Vertical axis shows model level with level 1 at top of model. Horizontal axis shows total wave number, n . Units and contouring are as in Fig. 3.

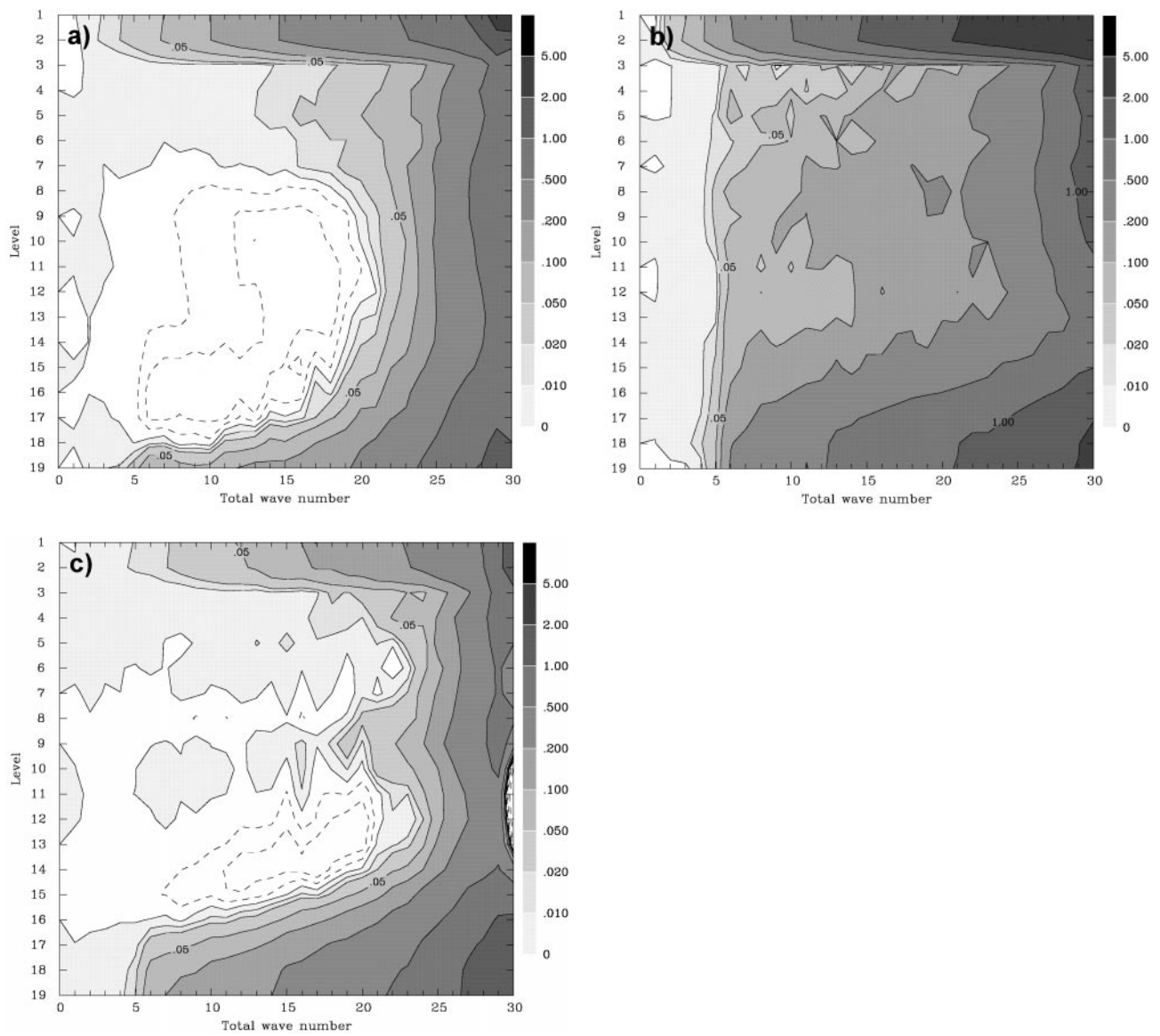


Fig. 5. As Fig. 4, but for ECHAM4 at T30 resolution and based on pairwise tendency errors of Runs 18-21 relative to Runs 14-17.

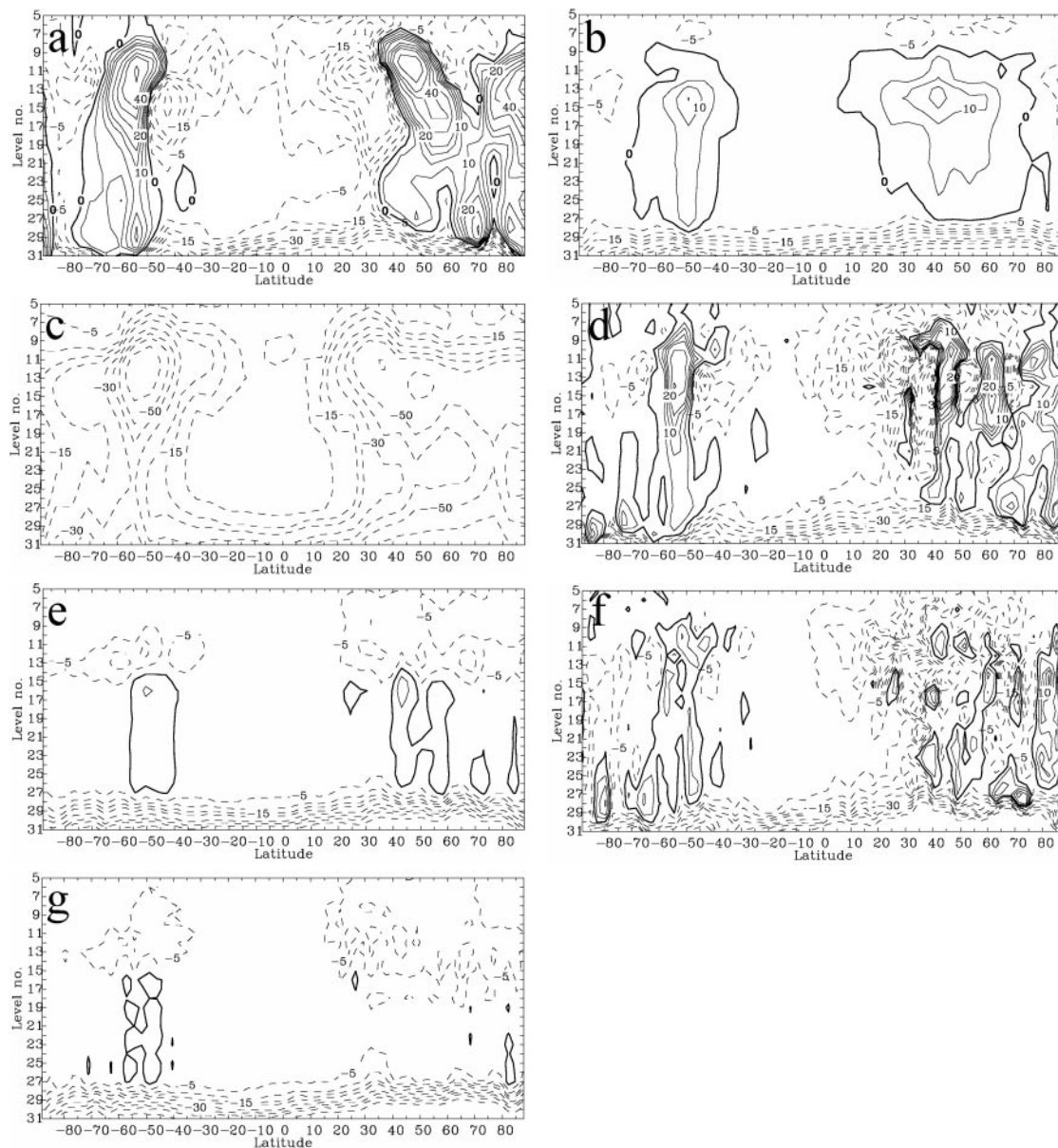


Fig. 6. Zonal and temporal average of generation of kinetic energy in ARPEGE/IFS due to unresolved scale interactions obtained a) from the tendency errors of Run 3 relative to Run 2, b) from the parameterised interaction term ($-\hat{h}_n \Psi_{n,m}(t)$) using the data from Run 2 and the T21 EIFs as in Fig. 4, c) from the standard T21-HF term ($-h_n \Psi_{n,m}(t)$) using the data from Run 2, d) from the tendency errors of Run 6 relative to Run 5, e) from the parameterised interaction term ($-\hat{h}_n \Psi_{n,m}(t)$) using the data from Run 5 and T30 EIFs f) from the tendency errors of Run 9 relative to Run 8, and g) from the parameterised interaction term ($-\hat{h}_n \Psi_{n,m}(t)$) using the data from Run 8 and T42 EIFs. Contour intervals at -70, -60, ..., -20, -15, -10, -5, 0, 5, 10, 15, 20, 30, ..., 70 $\text{m}^2 \text{s}^{-2} \text{day}^{-1}$.

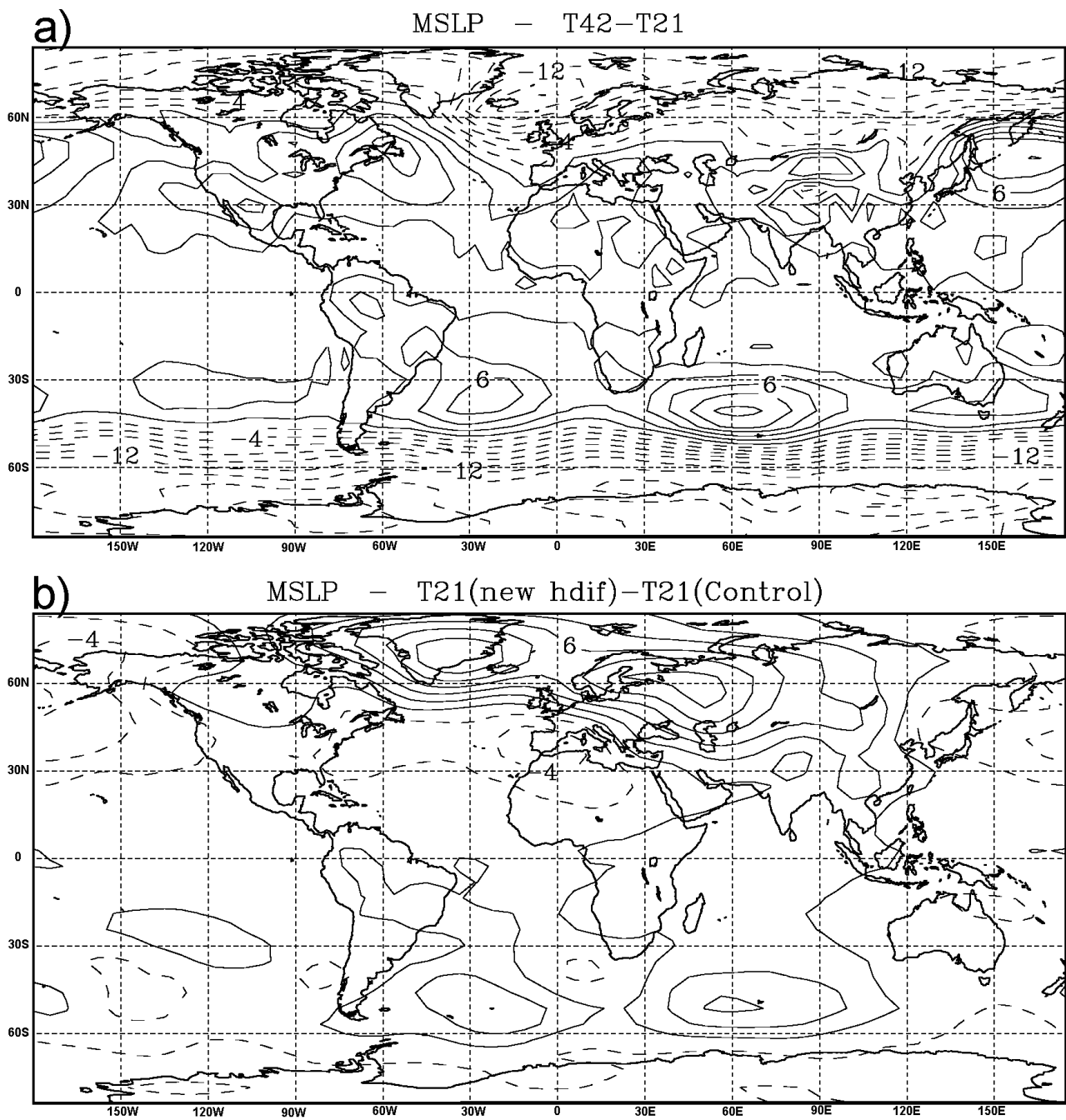


Fig. 7. Long term difference in mean sea level pressure between a) Run 26 (ARPEGE/T42) and Run 24 (ARPEGE/T21, original diffusion), and b) Run 25 (ARPEGE/T21, new diffusion) and Run 24 (ARPEGE/T21, original diffusion). Contour interval = 2 hPa.

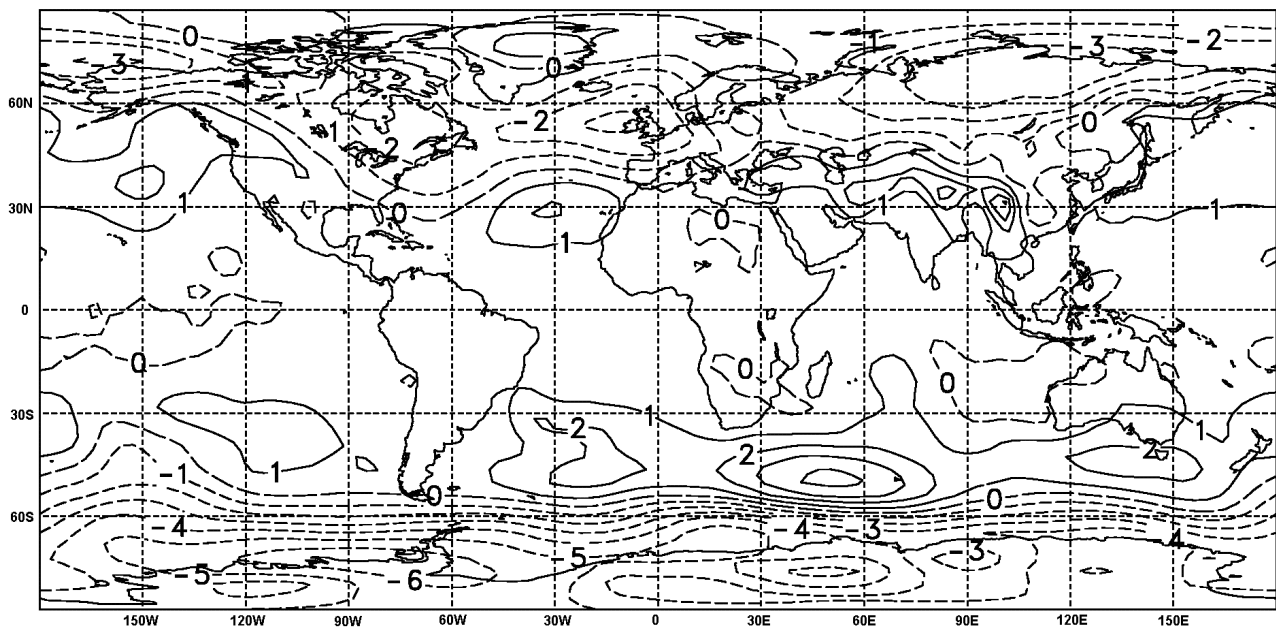


Fig. 8. Long term difference in mean sea level pressure between Run 22 (ECHAM4/T30, new diffusion) and Run 10 (ECHAM4/T30, original diffusion). Contour interval = 1 hPa. (note that the contour interval in Fig. 1 is 2 hPa).

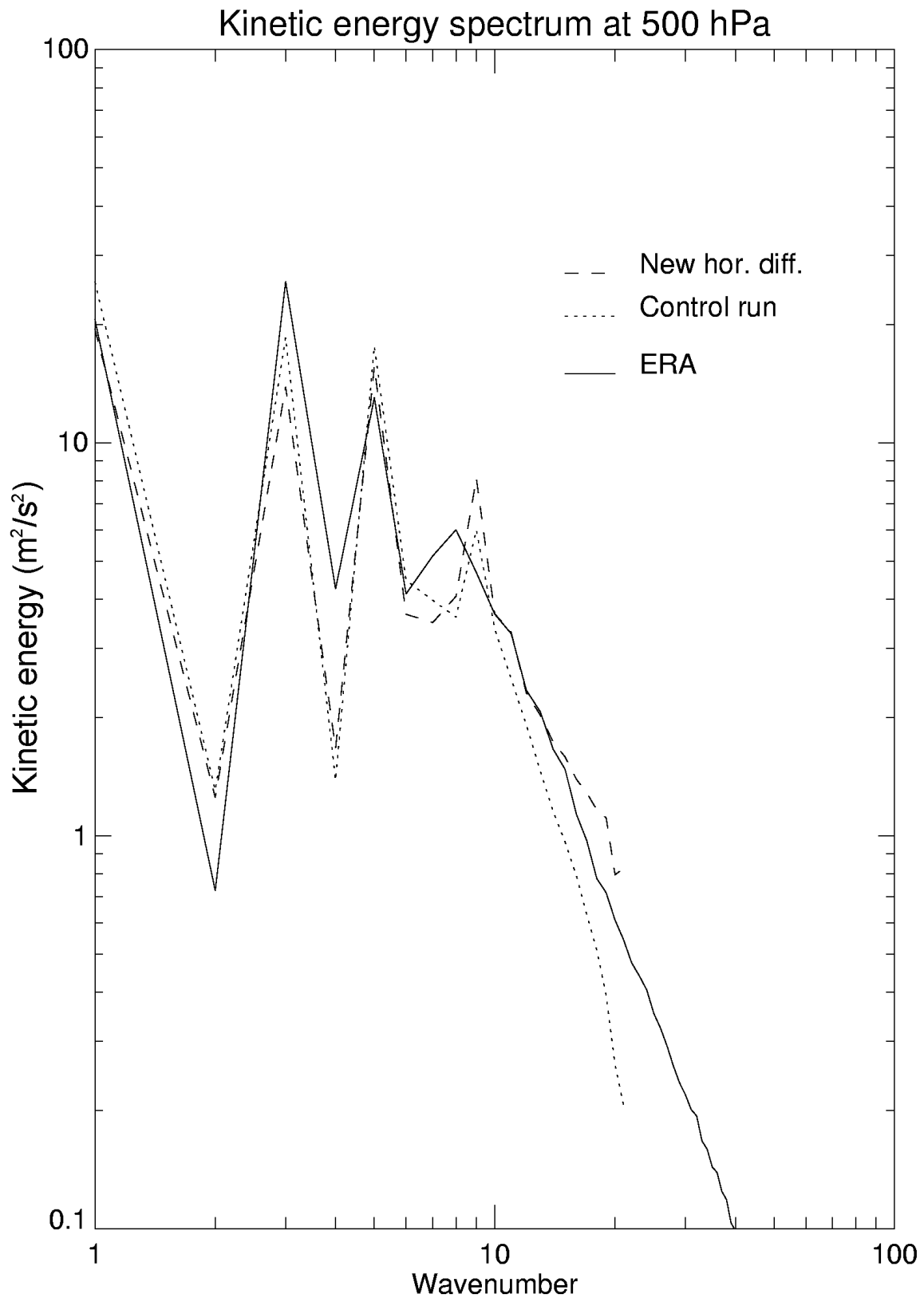


Fig. 9. Long term average of spectral density of kinetic energy at 500 hPa as function of total wave number (n) for ARPEGE/T21 control simulation (Run 24), stippled; for ARPEGE/T21 new diffusion (Run 25), dashed; and for ERA data in January full line.

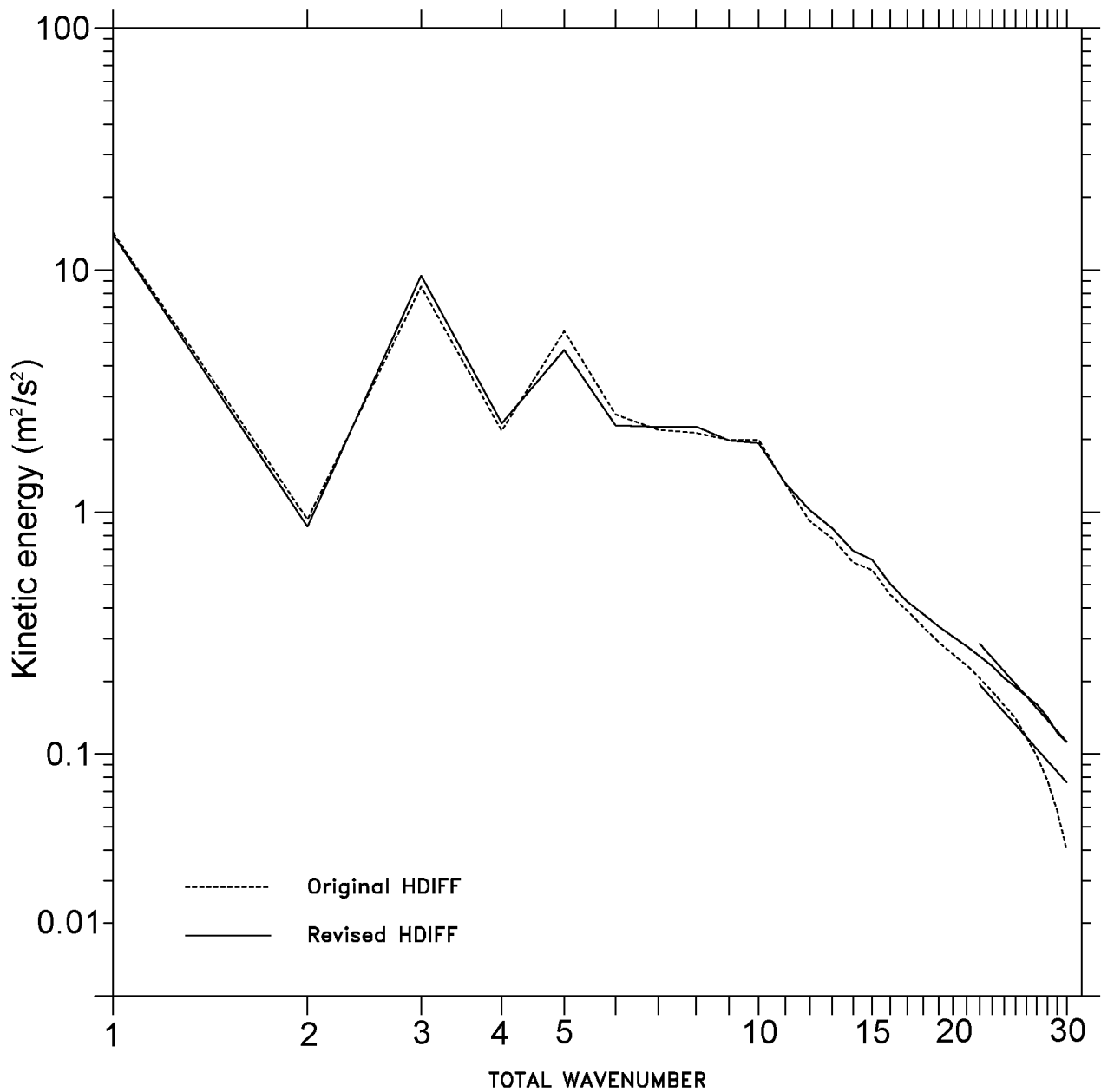


Fig. 10. As Fig. 9, but for ECHAM4/T30 control simulation (Run 10), stippled; and for ECHAM4/T30 new diffusion (Run 22), full line. At the end of each spectrum lines indicating the n^{-3} power law are shown.